

Flow-induced shear instabilities of cohesive granulates

Ilenia Battiato^{1,2,*} and Jürgen Vollmer^{2,3}

¹*Clemson University, Department of Mechanical Engineering, Clemson, SC 29634, USA*

²*Max Planck Institute for Dynamics and Self-Organization (MPIDS), 37077 Göttingen, Germany*

³*Fakultät für Physik, Universität Göttingen, 37077 Göttingen, Germany*

(Dated: 20 March 2012)

In this work we use a multi-scale framework to calculate the fluidization threshold of three-dimensional cohesive granulates under shear forces exerted by a creeping flow. A continuum model of flow through porous media provides an analytical expression for the average drag force on a single grain. The balance equation for the forces and a force propagation model are then used to investigate the effects of porosity and packing structure on the stability of the pile. We obtain a closed-form expression for the instability threshold of a regular packing of mono-disperse frictionless cohesive spherical grains in a planar fracture. Our result quantifies the compound effect of structural (packing orientation and porosity) and dynamical properties of the system on its stability.

PACS numbers: 45.70.-n, 45.05.+x, 62.20.M-, 47.56.+r, 47.55.nk

Keywords: Fluidization threshold; wet granulate; Brinkman equation; force network model; multiscale model; hydrodynamic force; instability

I. INTRODUCTION

Granulates are a large collection of macroscopic solid grains. Dry and wet granulates are vital in a large variety of industries, ranging from pharmaceutical to mining [1, pp. 4-10], from construction [2] to agricultural [1, pp. 10]. They also play an important role in many geological processes, such as land and mudslides [3], debris flows [4], erosion, particles re-suspension by wind in humid regions [5], and dune formation [6] that shape planets' morphology including, but not limited to, Earth [7].

Most theoretical and experimental studies focus on dry granulates and their collective behaviour including pattern formation [e.g., 7, 8], angle of stability/repose [e.g., 9, 10], avalanches dynamics [e.g., 11, 12] and granular flows [e.g., 13, 14]. However, as every child knows, adding even a small quantity of liquid to a sandpile dramatically changes its properties.

Cohesive interactions due to capillarity exist in three-phase systems such as partially-wet granulates where solid grains, wetting and non-wetting fluids (e.g. water and air) coexist. The existence of a *cohesive force* between grains leads to fundamentally different dynamics in wet granulates compared to their dry (i.e. non-cohesive) counterpart. Such differences include stability of granular piles and the location in a granular bed where incipient motion, either due to gravity [4, 15, 16] or shearing [e.g., 17–20], is first observed.

The collective behaviour of cohesive grains has only recently begun to be explored. A number of studies have focused on the dynamics of wet granular avalanches [e.g., 21] and on the effect of humidity [22–24] and capillary forces [15, 25, 26] on the static properties of granulates in both engineering applications [23] and natural systems, e.g. soil [27]. A number of different models have been proposed to

study the geometric stability of wet piles, including Mohr-Coulomb continuum [28], liquid-bridge [15] and response function [16, 29, 30] models.

While such models are invaluable in shedding light into the properties of *cohesive* granulates, natural systems often include a number of additional forcing factors that might significantly affect the stability of granulates in the environment. In geological systems, instability is triggered by a combination of body forces (e.g. gravity) and hydrodynamic shearing due to the creeping motion of a fluid through the granulate. This is especially true in processes such as cliff instability and landslides, sediment transport in submerged environments (e.g. seafloor transport), and fluidization of fines in fractures during pumping operations or oil recovery, just to mention a few. Even though the understanding of how flow-induced shear forces affect the stability of granular matter is of utmost importance to better quantify the processes that trigger a fluidization event, incorporating such effects is a challenging task since it requires the solution of Navier-Stokes equations in highly complex geometries.

In the present work we address this problem in a multi-scale framework and quantify the effect of dynamic shearing forces due to the creeping flow of a fluid (e.g. air) on the onset of instability (i.e. fluidization) of a cohesive granular pile (Fig. 1). Explicit analytical solutions are obtained for a model setting where the granulate is constituted of mono-disperse, frictionless, *cohesive* grains arranged in a regular packing. The cohesive interactions are due to the presence of capillary bridges formed by a wetting fluid, e.g. water, at the contact points between grains. Complications associated with random packing and friction between particles need not be taken into account to obtain reasonable results, as shown in [15].

In section II, we treat the cohesive granulate as a porous medium, and introduce a continuum-scale Darcy-Brinkmann model for the flow and the average drag force exerted by the fluid on the grains. Section III discusses a pore-scale network model for the force propagation through the pile. Location of failure and maximum load are derived. In section IV the

* ibattia@clemson.edu

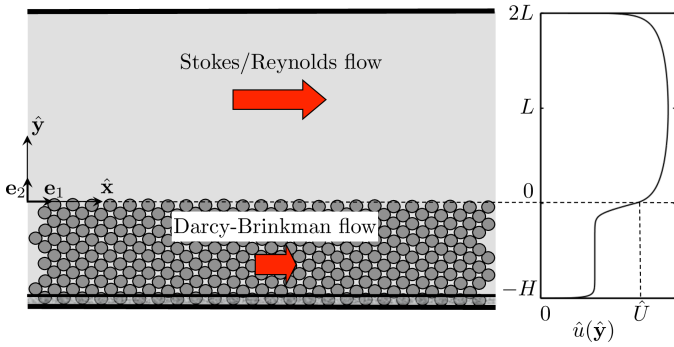


FIG. 1. Schematic of the domain on the left, and shape of the average velocity profile through the channel, on the right. The grains are assumed to be *cohesive*.

stability criterion is formulated in terms of the capillary number, that represents the relative strength between destabilising flow-induced shear and stabilising capillary (cohesive) forces, and the packing orientation relative to the average flow direction. The main results and conclusions are summarised in section V. For simplicity, gravity is here neglected. Generalisation to include gravity effects is straightforward.

II. CONTINUUM-SCALE MODEL OF FLOW AND DRAG IN A BRINKMAN MEDIUM

We consider a fully developed incompressible fluid flow, e.g. air, between two infinite parallel plates separated by the distance of $H + 2L$. The bottom part of the flow domain, $-H < \hat{y} < 0$, is occupied by a packing of cohesive (e.g. water-wet) mono-disperse rigid frictionless spheres of radius R . The (air) flow is driven by an externally imposed (mean) constant pressure gradient $d_{\hat{x}}\hat{p} < 0$. Therefore, each spherical grain is subject to a drag force due to aerodynamic stresses and attractive capillary bridge forces.

Since we are concerned with the fluidization threshold of the sphere packing, initially at rest, we treat the sphere-packed region as a porous medium with porosity ϕ and constant permeability K . This allows us to decouple an analysis of the flow from that of the granulate dynamics. We allow the flow over the granulate to span both laminar and turbulent regimes. Channel flow through, $\hat{y} \in (-H, 0)$, and over, $\hat{y} \in (0, 2L)$, a permeable layer can be described by coupling Brinkman with Navier-Stokes or Reynolds equation for the horizontal component $\hat{u}(\hat{y})$ of the average velocity $\hat{\mathbf{u}}(\hat{u}, \hat{v})$ [31, 32]

$$\mu_e d_{\hat{y}}\hat{u} - \mu K^{-1}\hat{u} - d_{\hat{x}}\hat{p} = 0 \quad \hat{y} \in (-H, 0), \quad (1a)$$

$$\mu d_{\hat{y}}\hat{u} - \rho\gamma d_{\hat{y}}\langle \hat{u}'\hat{v}' \rangle - d_{\hat{x}}\hat{p} = 0 \quad \hat{y} \in (0, 2L), \quad (1b)$$

where $d_{\hat{x}}\hat{p}$ is a mean constant pressure gradient, μ and ρ are the fluid's dynamic viscosity and density, respectively, and μ_e is its "effective" viscosity that accounts for the slip at the spheres walls. In the laminar regime ($\gamma = 0$), \hat{u} is the actual velocity and $\hat{v} \equiv 0$. In the turbulent regime ($\gamma = 1$), the actual velocity is decomposed into a mean velocity \hat{u} and velocity fluctuations \hat{u}' and \hat{v}' about their respective means.

$\langle \hat{u}'\hat{v}' \rangle$ denotes the Reynolds stress. Fully-developed turbulent channel flow has velocity statistics that depend on \hat{y} only.

In both laminar and turbulent regimes, the no-slip condition requires zero velocity at $\hat{y} = -H$ and $\hat{y} = 2L$, and the continuity of velocity and shear stress is prescribed at the interface, $\hat{y} = 0$, between the free and filtration flows [33]:

$$\hat{u}(-H) = \hat{u}(2L) = 0, \quad \hat{u}(0^-) = \hat{u}(0^+) = \hat{U}, \\ \mu_e d_{\hat{y}}\hat{u}|_{0^-} = \mu d_{\hat{y}}\hat{u}|_{0^+} \quad (2)$$

where \hat{U} is an unknown matching velocity at the interface between channel flow and porous medium.

Choosing (μ, H, q) , with $q = -\mu^{-1}H^2 d_{\hat{x}}\hat{p}$ a characteristic Darcy velocity, as the repeating variables, the problem can be formulated in dimensionless form. Then, inside the granular medium, the solution for the dimensionless velocity distribution $u = \hat{u}/q$ is given by [31]

$$u(y) = M^{-1}\lambda^{-2} + C_1 e^{\lambda y} + C_2 e^{-\lambda y}, \quad y \in (-1, 0), \quad (3a)$$

where $y = \hat{y}/H$, $M = \mu_e/\mu$, $\delta = L/H$, $\lambda^2 = H^2/(MK)$, and

$$C_{1,2} = \pm \frac{1}{M\lambda^2} \frac{(\lambda^2 U - 1)e^{\pm\lambda} + 1}{e^{\lambda} - e^{-\lambda}}, \quad (3b)$$

$$U = \frac{1}{\beta M\lambda^2} (1 - \text{sech}\lambda + \delta\lambda \tanh\lambda), \quad (3c)$$

with $U = \hat{U}/q$ the dimensionless interfacial velocity, and $\beta = 1$ or $\beta = 1 + (\tanh\lambda)/(2\delta M\lambda)$ for turbulent or laminar regime in the channel, respectively. In the following, we set $M = 1$ since the fluid does not experience any slip on the grains' walls.

The total drag on a sphere in an unbounded Brinkman medium is given by [34–36]

$$\hat{\mathbf{F}} = 6\pi\mu Rg(\phi)\hat{\mathbf{V}}, \quad (4)$$

where $\hat{\mathbf{V}}$ is a uniform velocity at infinity, $g(\phi) = 1 + \frac{3}{\sqrt{2}}(1 - \phi)^{1/2} + \frac{135}{64}(1 - \phi)\ln(1 - \phi) + 16.456(1 - \phi) + o(1 - \phi)$ [37, p.508, eq. (19.119)] and ϕ is porosity. Permeability, obtained by self-consistent arguments, is given by $K = k_s g^{-1}(\phi)$ [35, 36], where $k_s = \frac{2}{9}R^2(1 - \phi)^{-1}$ is the well-known Stokes result, for low-porosity packing of spheres. Since non-uniform velocity effects in Eq. (3a) are confined to a small region close to the upper and lower boundaries of the granulate, we employ a vertically averaged velocity $\bar{u}(y)$ to calculate a first-order approximation of the drag. Therefore, combining Eqs. (3a) and (4), the dimensionless drag force $\mathbf{F}(y) := (\mu q H)^{-1}\hat{\mathbf{F}} = [F(y), 0, 0] = F(y)\mathbf{e}_1$ exerted by the fluid on a sphere centered at y , is given by

$$F(y) = 3\pi\epsilon g(\phi)\bar{u}(y) \quad (5)$$

where $\epsilon = 2R/H$ is the dimensionless grain diameter, $\bar{u}(y) = \frac{1}{2\bar{h}} \int_{y-\bar{h}}^{y+\bar{h}} u(y') dy'$ is an average velocity across a layer of thickness $2\bar{h}$, and \mathbf{e}_1 is the unit vector in the x -direction.

In the following section we specialize the analysis to a regular (cubic) packing of spheres. This will allow us to determine the network of forces, and consequently the maximum load, developed inside the pile.

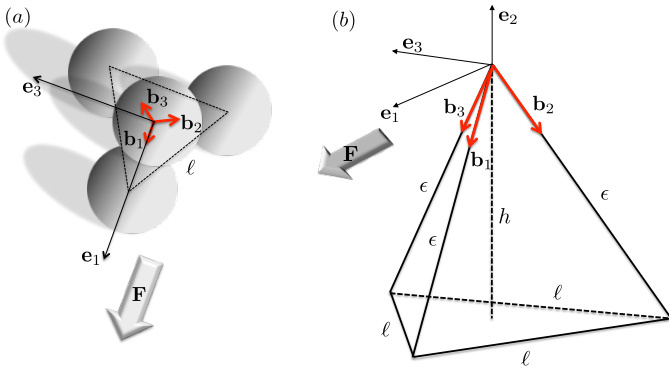


FIG. 2. (a) Top view of the structure of a two-layer 3-dimensional pile of spheres of dimensionless diameter ϵ . (b) Sketch of the tetrahedron obtained by connecting the centers of the 4-sphere structure (left). ℓ and h represent the intralayer and interlayer distances between sphere centers belonging to either the same or adjacent layers, respectively. \mathbf{e}_α , $\alpha = \{1, 2, 3\}$, are unit vectors of the canonical orthonormal basis of the Euclidean space. \mathbf{b}_α , $\alpha = \{1, 2, 3\}$, are unit vectors along the lattice directions connecting the center of the supported sphere with the centers of the supporting spheres.

III. FORCE NETWORK MODEL AND MAXIMUM LOAD

A. Geometry and packing

Let the mono-disperse cohesive grains be arranged in an isostatic packing, obtained by expanding a face-centered cubic packing so to eliminate interlayer contacts, with the (111)-face of the crystal parallel to the bottom wall of the channel. Such expanded packing configuration will be referred to as cubic expanded packing (CEP). From the first two layers of spheres (AB), a CEP arrangement can be obtained if every third layer is the same [38]. Figures 2(a) and (b) show the top and side views of the structure of the first two layers of spheres. While we focus on such a specific grains' arrangement, we stress that the analysis can be easily generalised to other regular packing structures. Let $\hat{\ell}$, with $2R < \hat{\ell} < 2\sqrt{3}R$, be the pitch in the $x - z$ (horizontal) plane, i.e. the distance between the centers of spheres belonging to the same layer, and \hat{h} the pitch in the $y - z$ (vertical) plane, i.e. the distance between two adjacent layers (Fig. 2). The dimensionless interlayer and intralayer distances $h = \hat{h}H^{-1}$ and $\ell = \hat{\ell}H^{-1}$, respectively, are related as follows $h = \epsilon[1 - \frac{1}{3}(\ell/\epsilon)^2]^{1/2}$. Porosity, ϕ , amounts to $\phi = 1 - \pi[3(\ell/\epsilon)^2\sqrt{3 - (\ell/\epsilon)^2}]^{-1}$, with $\epsilon < \ell < \sqrt{3}\epsilon$. When $\ell = \epsilon$ the close packing is recovered and $\phi \rightarrow \phi_c \approx 0.26$, corresponding to the face-centered cubic packing fraction of spheres, $s_c = \pi/3\sqrt{2} \approx 0.74$. If $\ell \rightarrow \sqrt{3}\epsilon$, $h \rightarrow 0$ and the four spheres lie on the same level.

Let $N + 1$ be the total number of layers in the pile. The bottom layer of grains is immobile and is called a *wall*. Therefore only N layers are mobile. Let $n = \{1, \dots, N\}$ denote the (mobile) layer number. The layer sitting immediately on the *wall* has $n = 1$. The layer enumeration continues moving up to the top-most layer in the pile where $n = N$ (see Fig. 3). The number of mobile layers, N , and the height of the pile,

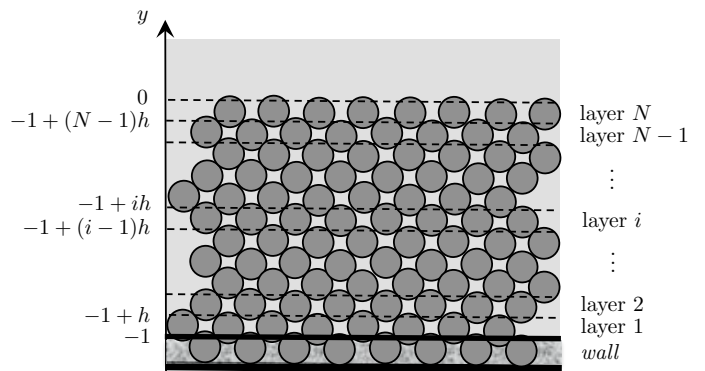


FIG. 3. Schematics of the layer enumeration. The dashed horizontal lines represent the location of the contacts between two adjacent layers of grains.

H , are related through $H = N\hat{h}$ or in terms of dimensionless quantities $N = 1/h$.

In the following section a pore-scale force network model is used to determine the location and the modulus of the maximum load in the pile.

B. Propagation of forces

Let \mathbf{F}_k be the sum of the external forces acting on grain k (e.g. drag), and $\mathbf{g}_{kl} = g_{kl}\mathbf{b}_{kl}$ the force exerted from grain k to grain l , where \mathbf{b}_{kl} is a unit vector pointing from grain k to grain l and g_{kl} is the magnitude of the force; g_{kl} is positive for compressive forces and negative otherwise. Whenever there is a stretched capillary bridge between two grains k and l , the force exerted by grain k on l is attractive and equal to a constant value $\mathbf{f}_{kl} = f_b\mathbf{b}_{kl}$ where $f_b > 0$. This simplifying assumption that the capillary force is a constant, irrespective of grain separation distance, has demonstrated to provide good description of collective behaviour of wet granulates [16, 39, 40]. The force distribution can be uniquely determined by solving the following system for the unknowns g_{kl}

$$\sum_l \mathbf{g}_{kl} = \mathbf{F}_k, \quad \forall k, l = 1, \dots, M, \quad (6)$$

with M the total number of grains. There is a unique solution for the force distribution [16, 29, 30] in d dimensions, if the packing is isostatic, i.e., if the average number ν of neighbours per grain equals $2d$. Note, however, that this solution does not necessarily comply with the constraint that contacts break when tensile forces exceed the capillary bridge force. Upon variation of parameters a regular packing yields when this additional requirement is first violated, i.e., the packing is stable as long as $g_{kl} + f_b > 0, \forall k, l$. Specifically, in a regular isostatic 3-dimensional CEP packing of grains bounded by a solid wall at the bottom and a free surface at the top each sphere is supported by $d = 3$ contacts from grains further down in the pile. For any couple (k, l) of grains in contact, the unit vector \mathbf{b}_{kl} connecting their centers is aligned to one of the (three) CEP-lattice directions. The external force (e.g. drag)

exerted on each grain up in the pile propagates unchanged down through the pile to the first mobile layer ($n = 1$) along such directions as discussed in [16]. Therefore, the maximum load is experienced from grains at the bottom of the pile, i.e. $n = 1$, and the stability threshold is determined by the respective bonds carrying the highest load. Next, we calculate the maximum destabilising force exerted on the lower-most grains in the pile.

C. Maximum load

From the continuum model solution, the average drag force $\mathbf{F}(n) = [F(n), 0, 0] = F(n)\mathbf{e}_1$ exerted by the fluid on a grain belonging to layer n can be obtained by setting the averaging interval in Eq. (5) equal to the layer thickness, i.e. $2\bar{h} = h$,

$$F(n) = \frac{3\pi\epsilon}{h}g(\phi) \int_{-1+(n-1)h}^{-1+nh} u(y)dy, \quad n = 1, \dots, N. \quad (7)$$

where $u(y)$ is given by Eq. (3). Therefore,

$$F(n) = \frac{3\pi\epsilon}{\lambda h}g(\phi) \left[\frac{h}{M\lambda} + C_1 e^{\lambda(-1+nh)} (1 - e^{-\lambda h}) + C_2 e^{\lambda(1-nh)} (1 - e^{\lambda h}) \right], \quad (8)$$

for $n = 1, \dots, N$, which gives the drag distribution due to aerodynamic shear exerted by the creeping fluid on the wet granular bed. The maximum load $\bar{\mathbf{F}}$, exerted on the grains of the first layer ($n = 1$), is

$$\bar{\mathbf{F}} = \sum_{n=1}^N \mathbf{F}(n). \quad (9)$$

Combining Eqs. (9) and (7) or (8) we obtain

$$\bar{\mathbf{F}} = \mathbf{e}_1 \frac{3\pi\epsilon}{h}g(\phi) \int_{-1}^0 u(y)dy, \quad (10)$$

which gives

$$\bar{\mathbf{F}} = \frac{3\pi\epsilon}{h}g(\phi)U_{\text{av}}\mathbf{e}_1, \quad (11)$$

where

$$U_{\text{av}} = \frac{1}{M\lambda^3} [\lambda + (M\lambda^2 U - 2)(\coth \lambda - \operatorname{csch} \lambda)], \quad (12)$$

is the average velocity across the granulate, and U is given by Eq. (3c) for laminar and turbulent regimes above the granulate.

IV. FLUIDIZATION THRESHOLD

While the maximum destabilizing average force $\bar{\mathbf{F}}$ on each grain in the bottom layer due to Stokes flow in the pile is parallel to the channel boundary, the stabilizing capillary forces act

along the lattice directions $\{\mathbf{b}_1, \mathbf{b}_2, \mathbf{b}_3\}$, see Fig. 2(b). Therefore, if the components of the total force $\bar{\mathbf{F}}$ along such directions are less than the capillary forces (assumed constant), the pile is stable: the stability criterion can be formulated by decomposing the force $\bar{\mathbf{F}}$ onto the non-orthogonal basis $\{\mathbf{b}_1, \mathbf{b}_2, \mathbf{b}_3\}$ uniquely identified by the structure of the packing.

In the following, we proceed with the non-orthogonal projection of the maximum load which allows us to analytically calculate the instability threshold while incorporating the impact of the lattice orientation relative to the average flow direction. We stress that such approach is readily generalizable to other packing structures and to incorporate any type of de/stabilizing forces (e.g. gravity, friction).

A. Non-orthogonal projection

Let $\mathcal{E} = \{\mathbf{e}_1, \mathbf{e}_2, \mathbf{e}_3\}$ be the canonical orthonormal basis of the Euclidean space \mathbb{R}^3 and $\mathcal{B} = \{\mathbf{b}_1, \mathbf{b}_2, \mathbf{b}_3\}$ a generally non-orthogonal basis with \mathbf{b}_α unit vectors, and $\alpha = \{1, 2, 3\}$. Let F_α be the components of the maximum force $\bar{\mathbf{F}}$ in the canonical basis, and F'_α its components in the basis \mathcal{B} , i.e.

$$\bar{\mathbf{F}} = \sum_{\alpha=1}^3 F_\alpha \mathbf{e}_\alpha = \sum_{\alpha=1}^3 F'_\alpha \mathbf{b}_\alpha. \quad (13)$$

The components of $\bar{\mathbf{F}}$ in the two basis are related through a linear transformation \mathbf{A} ,

$$(F_1, F_2, F_3) = \mathbf{A}(F'_1, F'_2, F'_3) \quad (14)$$

with (F_1, F_2, F_3) and (F'_1, F'_2, F'_3) column vectors, and \mathbf{A} the matrix of direction cosines whose components are defined as $A_{\alpha\beta} = \cos(\mathbf{b}_\beta, \mathbf{e}_\alpha) = \mathbf{b}_\beta \cdot \mathbf{e}_\alpha$.

In the \mathcal{B} -coordinate system and for any sphere belonging to the first mobile layer (i.e. $n = 1$), Eq. (6) simplifies to

$$F'_\alpha = f_b \quad \alpha = \{1, 2, 3\}, \quad (15)$$

and the stability criterion is

$$F'_\alpha \leq f_b, \quad \alpha = \{1, 2, 3\}. \quad (16)$$

Combining Eqs. (14) and (16) yields to

$$B_{\alpha\beta} F_\beta \leq f_b, \quad \alpha, \beta = \{1, 2, 3\}, \quad (17)$$

where $B_{\alpha\beta}$ are the components of $\mathbf{B} := \mathbf{A}^{-1}$. If the components of the maximum load F_β satisfy the system of (three) equations (17), then the pile is stable. Alternatively, Eq. (17) can be solved for the unknowns F_β , which provide the maximum magnitude of the components of the load that the capillary forces in the bottom layer can sustain.

The effect of the packing orientation on the pile stability can be readily incorporated. Without loss of generality, let us consider a counterclockwise rotation of the pile (and therefore of the basis \mathcal{B}) around the wall-normal, i.e. y -axis (see Figures 4 (a) and (b)). Such solid-body rotation is fully described by the rotation matrix $\mathbf{R}_y(\theta)$ defined as

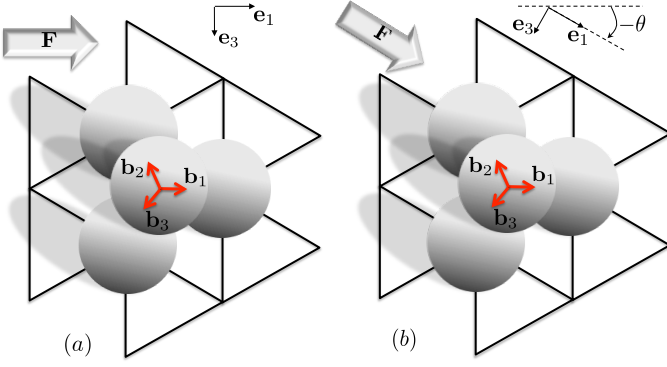


FIG. 4. Top view of the bottom two layers of a regular isostatic packing of mono-disperse spheres before (a) and after (b) a counterclockwise rotation θ of the packing.

$$\mathbf{R}_y(\theta) = \begin{bmatrix} \cos \theta & 0 & \sin \theta \\ 0 & 1 & 0 \\ -\sin \theta & 0 & \cos \theta \end{bmatrix} \quad (18)$$

where θ is the rotation angle. The matrix of direction cosines for the rotated system, \mathbf{A}_θ , is

$$\mathbf{A}_\theta = \mathbf{R}_y(\theta)\mathbf{A}. \quad (19)$$

The stability criterion, given by Eq. (16), now implies

$$B_{\theta,\alpha\beta}F_\beta \leq f_b \quad (20)$$

where $B_{\theta,\alpha\beta}$ are the components of $\mathbf{B}_\theta = (\mathbf{A}_\theta)^{-1}$, which gives a generalized stability criterion for an arbitrary orientation of the packing structure relative to the average direction of the aerodynamic drag.

B. Stability Diagram

Let us consider the Cartesian coordinate system as depicted in Fig. 1, where the axis \mathbf{e}_1 and \mathbf{e}_2 of the Cartesian basis \mathcal{E} are parallel and orthogonal to the fracture boundary. We take the projection of \mathbf{b}_1 onto the xz -plane parallel to \mathbf{e}_1 as a reference configuration for the packing orientation (Fig. 4(a)). Therefore, the components of the basis vectors $\{\mathbf{b}_1, \mathbf{b}_2, \mathbf{b}_3\}$ in the canonical basis \mathcal{E} and the matrix of direction cosines \mathbf{A} are

$$\mathbf{b}_1 = \frac{1}{\epsilon} \begin{bmatrix} \frac{\sqrt{3}}{3}\ell \\ -h \\ 0 \end{bmatrix}, \quad \mathbf{b}_2 = \frac{1}{\epsilon} \begin{bmatrix} -\frac{\sqrt{3}}{6}\ell \\ -h \\ -\frac{1}{2}\ell \end{bmatrix}, \quad \mathbf{b}_3 = \frac{1}{\epsilon} \begin{bmatrix} -\frac{\sqrt{3}}{6}\ell \\ -h \\ \frac{1}{2}\ell \end{bmatrix},$$

$$\mathbf{A} = \frac{1}{\epsilon} \begin{bmatrix} \frac{\sqrt{3}}{3}\ell & -\frac{\sqrt{3}}{6}\ell & -\frac{\sqrt{3}}{6}\ell \\ -h & -h & -h \\ 0 & -\frac{1}{2}\ell & \frac{1}{2}\ell \end{bmatrix}. \quad (21)$$

The matrix of direction cosines \mathbf{A}_θ after a counterclockwise rotation of angle θ about \mathbf{e}_2 -axis (Fig. 4 (b)) has the following components

$$[\mathbf{A}_\theta]_{ij} = \frac{1}{\epsilon} A_{\theta,ij} \quad (22)$$

where

$$\begin{aligned} A_{\theta,11} &= \frac{\sqrt{3}}{3}\ell \cos \theta, \\ A_{\theta,12} &= -\frac{\sqrt{3}}{6}\ell \cos \theta - \frac{\ell}{2} \sin \theta, \\ A_{\theta,13} &= -\frac{\sqrt{3}}{6}\ell \cos \theta + \frac{\ell}{2} \sin \theta, \\ A_{\theta,21} &= A_{\theta,22} = A_{\theta,23} = -h, \\ A_{\theta,31} &= -\frac{\sqrt{3}}{3}\ell \sin \theta, \\ A_{\theta,32} &= \frac{\sqrt{3}}{6}\ell \sin \theta - \frac{\ell}{2} \cos \theta, \\ A_{\theta,33} &= \frac{\sqrt{3}}{6}\ell \sin \theta + \frac{\ell}{2} \cos \theta. \end{aligned} \quad (23)$$

Therefore, combining the stability criterion, Eq. (20), with Eqs. (11), (22), and (23), we obtain the following system of equations

$$\begin{cases} \frac{2\sqrt{3}}{3} \left(\frac{\epsilon}{\ell}\right) F \cos \theta < f_b \\ -\frac{2\sqrt{3}}{3} \left(\frac{\epsilon}{\ell}\right) F \cos(\theta - \pi/3) < f_b, \\ -\frac{2\sqrt{3}}{3} \left(\frac{\epsilon}{\ell}\right) F \cos(\theta + \pi/3) < f_b \end{cases} \quad (24)$$

where $F = 3\pi\epsilon h^{-1}g(\phi)U_{av}$ is the total force exerted by the fluid and the pile on the first layer of grains ($n = 1$). The stability criterion, Eq. (24), can be re-written as

$$\begin{cases} 1 - \frac{2\sqrt{3}}{3}Ca^* \cos \theta > 0 \\ 1 + \frac{2\sqrt{3}}{3}Ca^* \cos(\theta - \pi/3) > 0, \\ 1 + \frac{2\sqrt{3}}{3}Ca^* \cos(\theta + \pi/3) > 0 \end{cases} \quad (25)$$

where Ca^* is a capillary number that incorporates geometrical effects of the porous structure and is defined as

$$Ca^* = \frac{p(\epsilon, \ell)U_{av}}{f_b}, \quad (26)$$

where $p(\epsilon, \ell) = 3\pi\epsilon^2g(\phi)/lh$ incorporates the impact of pore-scale geometry, and ϕ and h are uniquely determined for

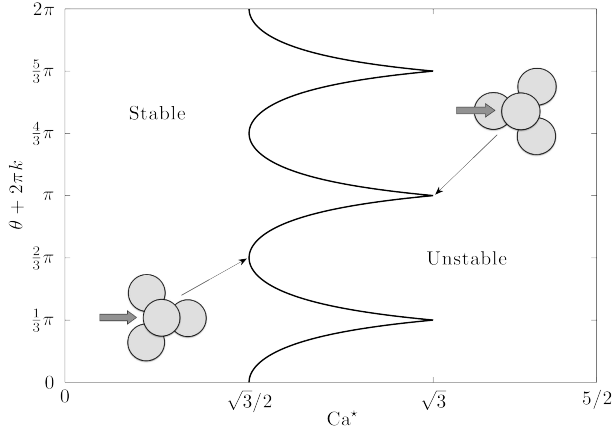


FIG. 5. Fluidization threshold of a wet granulate under flow-induced shear in terms of packing orientation θ and capillary number Ca^* .

any fixed (ϵ, ℓ) . Assuming a toroidal shape of the liquid surface of the capillary bridges, the dimensional capillary force $\hat{f}_b = \mu q H f_b$ can be related to the dimensional surface tension $\hat{\gamma} = \mu q \gamma$ and the contact angle between the wetting liquid (e.g. water) and the surface of the spheres η by

$$\hat{f}_b = 2\pi R \hat{\gamma} \cos \eta \quad (27)$$

[41, p. 190]. Therefore,

$$Ca^* = \frac{p'(\epsilon, \ell)}{\cos \eta} Ca, \quad (28)$$

where $p' = 3\epsilon g/(\ell h)$ and $Ca = \mu \hat{U}_{av}/\hat{\gamma}$ is the capillary number defined in terms of the average velocity \hat{U}_{av} . Solving Eq. (25) leads to the following stability criterion for the CEP as a function of packing orientation θ and capillary number Ca^* ,

$$\left\{ \begin{array}{ll} Ca^* < \frac{\sqrt{3}}{2}, & \text{stable} \quad \forall \theta \\ Ca^* > \sqrt{3}, & \text{unstable} \quad \forall \theta \\ Ca^* \in (\frac{\sqrt{3}}{2}, \sqrt{3}), & \text{stable if } \theta \in [\arccos(\sqrt{3}/2Ca^*), \frac{2}{3}\pi - \arccos(\sqrt{3}/2Ca^*)] \end{array} \right. \quad (29)$$

A graphical representation of Eq. (29) is provided in Figure 5. The stability of a pile with CEP arrangement of its grains is affected by the orientation of the lattice directions relative to the average velocity of the flow by a factor of 2 (Fig. 5): the pile orientation determines how the destabilising hydrodynamic forces decompose along the lattice directions and, consequently, how they are balanced by the stabilising capillary forces acting at the contact points. Combining Eqs. (26) and (27), Ca^* can be written as follows

$$Ca^* = \left(\frac{3\mu\epsilon^2 g(\phi)}{2\hat{\gamma}\ell h \cos \eta} \right) \frac{H}{R} \hat{U}_{av} \quad (30)$$

Besides the geometrical arrangement and the physical properties of the wetting and non-wetting fluids (first parenthesis on the RHS), two relevant parameters that control the fluidization threshold are the average velocity across the granulate and the number of layers, since Ca^* is proportional to H/R . While filtration velocities in low permeability porous media are generally very small, scale effects play a crucial role in determining whether or not flow-induced shear might become a significant source of instability of unconsolidated cohesive granulates.

V. SUMMARY AND CONCLUSIONS

In many environmental and industrial systems, the instability of cohesive granulates is triggered by a combination of body (e.g. gravity), surface (e.g. friction) and (boundary and/or flow-induced) shearing forces. Flow-induced shear forces represent an important instability factor in many systems where fluid flow occurs, e.g. cliff instability after heavy rainfall, sediment transport in submerged environments, and pumping operations during oil recovery, just to mention a few. While a number of works have focused on the effect of friction, gravity and boundary shearing on cohesive granulates instability, studying the impact of flow-induced shear forces represents a major challenge since it would a priori require the full (numerical) solution of Navier-Stokes equations in highly complex geometry for drag computation.

In this work we use a multi-scale framework to account for the effect of fluid dynamic shearing on the stability of cohesive granulates. We provide closed-form expressions for the instability threshold, due to flow-induced shear forces, of a regular packing of cohesive mono-disperse spherical grains in a planar fracture. Without loss of generality, the analysis is specialised to cohesive forces of capillary nature. In this setting, the compound effect of structural (e.g. porosity, grain contacts distribution, pile orientation) and dynamical (e.g. capillary and fluid-dynamics forces) properties of the system on its stability is taken into account. The impact of packing orientation is also quantified: the orientation of a CEP pile affects its stability threshold by a factor of 2. Moreover, we identify the capillary number, Ca^* , Eq. (26), as the dimensionless parameter that controls the instability threshold. Ca^* is the ratio between destabilizing fluid dynamic shear forces and stabilizing cohesive (capillary) forces, given by Eqs. (10) and (27), respectively. It is defined in terms of the average shearing velocity \hat{U}_{av} , the fluid viscosity μ , the surface tension $\hat{\gamma}$, the geometrical arrangement of the grains, the contact angle η between wetting liquid and the surface of the solid grains, and the ratio between the height of the pile H and the typical grain diameter R . This implies that even though filtration velocities might be very small, creeping flow might play a key role in the instability of unconsolidated cohesive granulates due to scale effects. We stress that, while applied to cohesive capillary forces, the method can also be used to model any type of cohesive forces (e.g. Van der Waals). Generalisation to include gravity and/or friction is also straightforward.

Idealized systems as those considered in this study can pro-

vide interesting insights on the salient features, for example, location of failure, and relevant parameters controlling cohesive granulates instabilities induced by fluid shear. Also, since regularly arranged monodisperse granulates lead to a uniform distribution of the loads, their instability threshold might provide a sufficient condition for the instability of similarly loaded/sheared disordered packings where the load is highly localized to fewer force chains bearing a higher maximum load.

Real systems, on the other hand, exhibit a host of additional features including grains polydispersity in size and shape, additional forcing factors (e.g., gravity, friction, nonuniform distribution of cohesive forces), and fluid anomalous rheology (i.e., non-Newtonian behavior). These affect the force balance at both a local and global level due to structural changes of the force network and contact loads distribution. In random packings, the latter is highly anisotropic and inhomogeneous due to the presence of force chains that bear most of the load. While such inhomogeneity might potentially induce significant deviations from the behavior of cohesive granulates with a regular arrangement of grains, it has been shown that analysis/predictions based upon regular arrangements of frictionless monodisperse spheres provide remarkably good predictions concerning the stability properties of nonspherical randomly packed frictional granulates [15]. This might be attributed to the observed constant mechanical strength of randomly packed wet granulates over a wide range of wetting liquid contents [41]. Scheel et al. [41] theoretically derived the cohesivity of randomly packed glass beads by approximating them with uniform arrangements of frictionless spheres. Their experiments on both monodisperse and polydisperse sand grains led to a remarkably good match with their theoretical predictions. It has been therefore speculated that roughness, as well as randomness, might play only a secondary role in determining the static and dynamic properties of random polydisperse granulates [42]. Fully quantitative investigations on random (polydisperse) granulates are therefore needed to elucidate such mechanisms.

The study of contact loads distribution in random networks related to the onset of instability poses significant additional analytical challenges since it requires the evaluation of loads spatial distribution. More importantly, the tails of such distributions have to be evaluated since they are associated to the maximum loads, which drive the global instability of the system. While analytical probability density function (pdf) methods might be employed to obtain the full pdf of the contact loads, load redistribution to surviving chains after local rupture could be addressed by, for example, random fiber bundle model [43]. A combination of such analytical and numerical methods could represent an alternative to computationally intensive full molecular dynamics simulations. In addition, many fluids in natural, industrial, and biological systems exhibit non-Newtonian behavior (e.g., oil, paints, blood). Anomalous rheology of the flowing fluid dramatically affects the macroscopic behavior of the system, its governing equations, and the stress distribution inside the granulate due to the nonlinear coupling between pore-space geometry and the rheological properties of the fluid [44]. Nevertheless, it has been showed that power-law fluids exhibit universality behavior, and that their flow properties might belong to the same universality class of Newtonian fluid flows [44]. This suggests that the approach employed in our study could be easily generalized to non-Newtonian fluids. The application of pdf methods to randomly packed cohesive granulates instability will be object of future investigations, together with the study of regular packing structures other than cubic (e.g., arrangements derived from hexagonal close packing), size and density polydispersity, and the effect of fluid non-Newtonicity.

ACKNOWLEDGMENTS

Funding from BP International within the ExploRe program is gratefully acknowledged.

-
- [1] J. Duran, *Sands, Powders, and Grains* (Springer-Verlag, New York, USA, 2000).
 - [2] S. Watano, Y. Imada, K. Hamada, Y. Wakamatsu, Y. Tanabe, R. N. Dave, and R. Pfeffer, *Powder Technol.* **131**, 250 (2003).
 - [3] R. Dikau and D. Brunsten, *Landslide Recognition: Identification, Movement and Causes* (John Wiley & Sons, London, UK, 1996).
 - [4] R. M. Iverson, M. E. Reid, N. R. Iverson, R. G. LaHusen, M. Logan, J. E. Mann, and D. L. Brien, *Science* **290**, 513 (2000).
 - [5] K. W. Nicholson, *Atmos. Environ.* **22**, 2639 (1988).
 - [6] R. A. Bagnold, *The Physics of Blown Sand and Desert Dunes* (Methuen, London, UK, 1941).
 - [7] C. Hansen, M. Bourke, N. Bridges, S. Byrne, C. Colon, S. Diniega, C. Dundas, K. Herkenhoff, A. McEwen, M. Mellon, et al., *Science* **331**, 575 (2011).
 - [8] P. Umbanhowar, F. Melo, and H. Swinney, *Nature* **382**, 793 (1996).
 - [9] H. M. Jaeger, C. L. Liu, and R. Nagel, *Phys. Rev. Lett.* **62**, 40 (1989).
 - [10] J. J. Alonso and H. J. Herrmann, *Phys. Rev. Lett.* **76**, 4911 (1996).
 - [11] P. Jop, Y. Forterre, and O. Pouliquen, *Nature* **441**, 727 (2006).
 - [12] P. Jop, Y. Forterre, and O. Pouliquen, *Phys. Fluids* **19**, 088102 (2007).
 - [13] J. Rajchenbach, *Phys. Rev. Lett.* **90**, 144302 (2003).
 - [14] G. MiDi, *Eur. Phys. J. E* **14**, 341 (2004).
 - [15] S. Novak, A. Samadani, and A. Kudrolli, *Nature Phys.* **1**, 50 (2005).
 - [16] S. H. Ebrahimpazhad-Rahbari, J. Vollmer, S. Herminghaus, and M. Brinkmann, *EPL* **87**, 14002 (2009).
 - [17] F. Charru and H. Mouilleron-Arnould, *J. Fluid Mech.* **452**, 303 (2002).
 - [18] H. Mouilleron, F. Charru, and O. Eiff, *J. Fluid Mech.* **628**, 229 (2009).
 - [19] M. Ouriemi, P. Aussillous, and E. Guazzelli, *J. Fluid Mech.*

- 636**, 295 (2009).
- [20] S. H. E. Rahbari, J. Vollmer, S. Herminghaus, and M. Brinkmann, *Phys. Rev E* **82**, 061305 (2010).
- [21] P. Tegzes, T. Vicsek, and P. Schiffer, *Phys. Rev. E* **67**, 051303 (2003).
- [22] N. Fraysse, H. Thomé, and L. Petit, *Eur. Phys. J. B* **11**, 615 (1999).
- [23] K. Fray and C. Marone, *J. Geophys. Res.* **107**, 2309 (2002).
- [24] F. Restagno, C. Ursini, H. Gayvallet, and E. Charlaix, *Phys. Rev. E* **66**, 021304 (2002).
- [25] D. J. Hornbaker, R. Albert, I. Albert, A.-L. Barabási, and P. Schiffer, *Nature* **387**, 765 (1997).
- [26] F. Restagno, L. Bouquet, and E. Charlaix, *Eur. Phys. J. E* **14**, 177 (2004).
- [27] R. M. Iverson, *Water Resour. Res.* **36**, 1897 (2000).
- [28] T. G. Mason, A. J. Levine, D. Ertas, and T. C. Halsey, *Phys. Rev. E* **60**, R5044 (1999).
- [29] C. Moukarzel, *Phys. Rev. Lett.* **81**, 1634 (1998).
- [30] C. Moukarzel, *Response Functions in Isostatic Packings* (The Physics of Granular Media, Wiley-VCH Verlag, 2004).
- [31] I. Battiato, P. R. Bandaru, and D. M. Tartakovsky, *Phys. Rev. Lett.* **105**, 144504 (2010).
- [32] I. Battiato, *J. Fluid Mech.* (in press) (2012).
- [33] K. Vafai and S. J. Kim, *Int. J. Heat and Fluid Flow* **11**, 254 (1990).
- [34] S. Kim and W. B. Russel, *J. Fluid Mech.* **154**, 269 (1985).
- [35] I. D. Howells, *J. Fluid Mech.* **64**, 449 (1974).
- [36] E. J. Hinch, *J. Fluid Mech.* **83**, 695 (1977).
- [37] S. Torquato, *Random Heterogenous Material - Microstructure and Macroscopic Properties* (Springer, New York, USA, 2000).
- [38] N. W. Ashcroft and N. D. Mermin, *Solid State Physics*, ISBN-13: 978-0030493461 (Saunders College Publ., Philadelphia, 1976).
- [39] A. Fingerle, K. Roeller, K. Huang, and S. Herminghaus, *New J. Phys.* **10**, 053020 (2008).
- [40] S. Ulrich, T. Aspelmeier, K. Roeller, A. Fingerle, S. Herminghaus, and A. Zippelius, *Phys. Rev. Lett.* **102**, 148002 (2009).
- [41] M. Scheel, R. Seemann, M. Brinkmann, M. di Michiel, A. Sheppard, B. Breidenbach, and S. Herminghaus, *Nature Mater.* **7**, 189 (2008).
- [42] A. Kudrolli, *Nature Mater.* **7**, 174 (2008).
- [43] F. Dalton, A. Petri, and G. Pontuale, *J. Stat. Mech.* (2010), P03011.
- [44] A. F. Morais, H. Seybold, H. J. Herrmann, and J. S. Andrade, *Phys. Rev. Lett.* **103**, (2009), 194502.